Inorganic Chemistry

Article

Electron Transfer and Ligand Addition to Atomic Mercury Cations in the Gas Phase: Kinetic and Equilibrium Studies at 295 K

Xiang Zhao, Eric Flaim, Lise Huynh, Michael J. Y. Jarvis, Ping Cheng, Vitali V. Lavrov, Voislav Blagojevic, Gregory K. Koyanagi, and Diethard K. Bohme*

Department of Chemistry, Centre for Research in Mass Spectrometry and Centre for Research in Earth and Space Science, York University, Toronto, Ontario, Canada M3J 1P3

Results are reported for experimental measurements of the room-temperature chemical reactions between ground-state $Hg^{\bullet+}$ ions and 16 important environmental and biological gases: SF_6, CO, CO_2, N_2O, D_2O, CH_4, CH_3F, O_2, CH_3Cl, OCS, CS_2, NH_3, C_6F_6, NO_2, $NO^\bullet$, and C_6H_6. The inductively coupled plasma/selected-ion flow tube tandem mass spectrometer used for these measurements has provided both rate and equilibrium constants. Efficient electron transfer (>19%) is observed with CS_2, NH_3, C_6F_6, NO_2, $NO^\bullet$, and C_6H_6, molecular addition occurs with D_2O, CH_4, CH_3F, CH_3Cl, and OCS, and SF_6, CO, CO_2, N_2O, and O_2 showed no measurable reactivity with $Hg^{\bullet+}$. Theory is used to explore the stabilities and structures of both the observed and unobserved molecular adducts of $Hg^{\bullet+}$, and reasonable agreement is obtained with experimental observations, given the uncertainties of the theory and experiments. A correlation is reported between the $Hg^{\bullet+}$ and proton affinities of the ligands investigated. Solvation of $Hg^{\bullet+}$ with formic acid was observed to increase the rate of electron transfer from $NO^\bullet$ by more than 20%.

1. Introduction

Studies of chemical reactions of mercury cations in the gas phase date back to at least 1967 when efforts were made to develop a mercury-plasma bridge neutralizer to use with a mercury thruster for the electric propulsion of ion engines into space.[1−3] The relative merits of Hg and Cs as neutralizers were evaluated with measurements of the electron-transfer reaction of $Hg^{\bullet+}$ with Cs at high energies (1−15 keV). Thermal reactions of $Hg^{\bullet+}$ with molecules appear not to have been investigated until 1976 during the early days of ion cyclotron resonance (ICR) mass spectrometry when Allison and Ridge reported the formation of HgI^+, rather than the methyl-mercury cation $HgCH_3^+$, from the reaction of $Hg^{\bullet+}$ with CH_3I.[4] $Hg^{\bullet+}$ and $HgBr^+$ cations were generated in a low-voltage DC discharge containing CH_3HgBr and used for chemiluminescent studies of these cations.[5] Further qualitative studies, this time using FT-ICR, were reported in 1994 for reactions of $Hg^{\bullet+}$ produced by laser ablation of red

mercury(II) sulfide.[6] Reactions were observed with benzene and several substituted benzenes, several arylthiols, and two butylthiols, and these were dominated by electron transfer. An interesting near-resonant electron-transfer reaction with H_2S also was observed. Electron transfer to $Hg^{\bullet+}$ also has been reported with dimethyl peroxide; here $Hg^{\bullet+}$ was produced by laser ablation of an alloy of tin, silver, and mercury.[7] Finally, the electron transfer from Ar or Kr to doubly charged Hg^{2+} cations[7] and the mobility of these cations in helium have been investigated at low collision energies using the flow drift tube technique.[8,9]

Overall, reported studies of the chemistry of bare $Hg^{\bullet+}$ have been surprisingly sparse, and apparently, no quantitative information was available on the *room-temperature* kinetics of this chemistry until we began to employ our recently constructed ICP/SIFT tandem mass spectrometer. We reported the room-temperature kinetics of the reactions of $Hg^{\bullet+}$ ($5d^{10}6s^1$) with N_2O, O_2, and C_6F_6 in early applications of

---

* To whom correspondence should be addressed. E-mail: dkbohme@yorku.ca.

(1) Daley, H. L.; Perel, J. *AIAA J.* **1969**, *7*, 733−734.
(2) Rawlin, V. K.; Pawlik, E. V. *AIAA* **1967**, *Paper 67−671*.
(3) Hall, D. F.; Kemp, R. E.; Shelton, H. *AIAA* **1967**, *Paper 67−670*.
(4) Allison, J.; Ridge, D. P. *J. Am. Chem. Soc.* **1976**, *98*, 7445−7447.
(5) Michael, A.; Kushawaha, V. *J. Phys. B: At., Mol. Opt. Phys.* **1989**, *22*, 3255−3267.

(6) El-Nakat, J. H.; Dance, I. G.; Fisher, K. J.; Willett, G. D. *Polyhedron* **1994**, *13*, 409−415.
(7) Wesendrup, R.; Schalley, C. A.; Schröder, D.; Schwarz, H. *Chem.− Eur. J.* **1995**, *1*, 608−613.
(8) Hansel, A.; Richter, R.; Lindinger, W.; Herman, Z. *Int. J. Mass Spectrom. Ion Processes* **1992**, *117*, 213−222.
(9) Hansel, A.; Richter, R.; Herman, Z.; Lindinger, W. *J. Chem. Phys.* **1991**, *94*, 8632−8633.

this new instrument. No reaction was observed with N_2O ($k \leq 10^{-13}$ cm^3 molecule^{-1} s^{-1}).[10] The reaction with O_2 was reported to be very slow and to produce the adduct ion Hg^+O_2 ($k = 2.4 \times 10^{-13}$ cm^3 molecule^{-1} s^{-1}).[11] C_6F_6 was measured to transfer an electron to $Hg^{\bullet+}$ with unit efficiency and $k = 7.4 \times 10^{-10}$ cm^3 molecule^{-1} s^{-1}.[12]

Since mercury has the highest ionization energy among the metallic elements of the periodic table, IE(Hg) = 10.44 eV,[13] atomic mercury cations are more prone than other atomic metal cations to react at thermal energies by electron transfer. Here we explore the efficiency of electron transfer with various molecules having ionization energies in the range from 9.2 to 15.3 eV. With one reagent molecule, NO$^\bullet$, we had the opportunity to explore the influence of solvation with formic acid on the occurrence of electron transfer to $Hg^{\bullet+}$. Furthermore, we also explore, and in some cases report equilibrium constant measurements of, the tendency of molecules to attach to $Hg^{\bullet+}$ when electron transfer is endothermic. Our observations of a number of $Hg^{\bullet+}$ adduct ions raise questions about their structure, and we have investigated these using DFT calculations. Altogether, we report here experimental measurements of gaseous reactions between $Hg^{\bullet+}$ and 16 important environmental and biological gases (SF_6, CO, CO_2, N_2O, D_2O, CH_4, CH_3F, O_2, CH_3Cl, OCS, CS_2, NH_3, C_6F_6, NO_2, NO$^\bullet$, and C_6H_6). The results provide extensive new insights into the intrinsic chemical reactivity of this important environmental and biological metal-radical cation.

2. Experimental Section

The kinetic and equilibrium measurements were taken with an inductively coupled plasma/selected-ion flow tube (ICP/SIFT) tandem mass spectrometer. The SIFT apparatus and ICP ion source, as well as the ICP/SIFT interface, have been described previously.[14−17] $Hg^{\bullet+}$ ions were generated in the ICP source by spraying a dilute (5 μg mL^{-1}) solution of Hg in hydrochloric acid and water. $Hg^{\bullet+}$ ions emerging from the ICP source were mass analyzed with a quadrupole mass filter and injected into a stainless steel flow tube that is continuously flushed with helium buffer gas at a steady-state pressure of 0.35 ± 0.01 Torr and 295 ± 2 K. At the operating temperature of the argon plasma estimated to be 5500 K, the $Hg^{\bullet+}$ is produced primarily (99.97%) in the ^2S (5d^{10} 6s) ground electronic state.[10] The helium buffer gas in the flow tube acts to thermalize the kinetic energy of the $Hg^{\bullet+}$ ions by collisions with He atoms so that they reach a temperature prior to reaction equal to the tube temperature of 295 ± 2 K.

Reagent gases and vapors were introduced in the flow tube through an inlet tube. Some were added as solutions in helium (10−20%). All were of high purity (>99%).

Further downstream, a second quadrupole mass filter was used to monitor the intensities of reactant and product ions as a function of the flow of the neutral reagent. Rate coefficients for the primary reactions of all ions present in the system are determined with an uncertainty of $\pm 30\%$ from the rate of decay of the reactant ion intensity using pseudo-first-order kinetics. Higher-order rate coefficients are obtained by fitting the experimental data to the solutions of the system of differential equations for sequential reactions.[14,15]

Equilibrium constants for ligation reactions were determined at the fixed reaction time (9.4 ms) of our experiment from a plot of the ion signal ratio or ion concentration ratio, [Hg$^{\bullet+}$L]/[Hg$^{\bullet+}$], against the flow of ligand L when this plot becomes linear and mass discrimination is taken into account. Only lower limits to the equilibrium constants are accessible when equilibrium is not achieved in the reaction region either because of insufficient time or because of a fast sequential addition to form a more highly ligated cluster which prevents sufficient back reaction. Equilibrium is not achieved when the ion signal ratio plot does not achieve linearity in the reactant flow range of the experiment (the last point of the curved plot will then provide a lower limit). Alternatively, further reaction of the product cluster may prevent the achievement of linearity and cause downward curvature before the achievement of linearity (in this case, the tangent to the onset of curvature provides a lower limit to K). Equilibrium also is not achieved for reactions with very large equilibrium constants or with reagent vapors such as water vapor that cannot be added in large enough amounts. Breakup of the adduct ion in the sampling process also will lead to lower limits for the true equilibrium constant. However, this latter effect will be most pronounced for the weakest bonds and should not be an issue for adduct ions with binding free energies ≥ 5 kcal mol^{-1}.

3. Theoretical Section

All quantum chemistry calculations in this paper are performed with the B3LYP hybrid density functional method[18,19] and achieved with the GAUSSIAN98 suite of programs.[20] In all cases, the thermochemistry calculated here is corrected for zero-point energy (ZPE) effects. The 6-311++G(d, p) basis set[21,22] is used for all of the elements except Hg, for which the LANL2DZ[23−25] basis set was used. All stationary points were characterized by harmonic vibrational frequency calculations and these established that all the

(10) Lavrov, V. V.; Blagojevic, V.; Koyanagi, G. K.; Orlova, G.; Bohme, D. K. *J. Phys. Chem. A* **2004**, *108*, 5610−5624.

(11) Koyanagi, G. K.; Caraiman, D.; Blagojevic, V.; Bohme, D. K. *J. Phys. Chem. A* **2002**, *106*, 4581−4590.

(12) Caraiman, D.; Koyanagi, G. K.; Bohme, D. K. *J. Phys. Chem. A* **2004**, *108*, 978−986.

(13) NIST Chemistry WebBook, NIST Standard Reference Database Number 69, http://webbook.nist.gov/chemistry/.

(14) Mackay, G. I.; Vlachos, G. D.; Bohme, D. K.; Schiff, H. I. *Int. J. Mass Spectrom. Ion Phys.* **1980**, *36*, 259−270.

(15) Raksit, A. B.; Bohme, D. K. *Int. J. Mass Spectrom. Ion Processes* **1983**, *55*, 69−82.

(16) Koyanagi, G. K.; Lavrov, V. V.; Baranov, V.; Bandura, D.; Tanner, S.; McLaren, J. W.; Bohme, D. K. *Int. J. Mass Spectrom.* **2000**, *194*, L1-L5.

(17) Koyanagi, G. K.; Baranov, V. I.; Tanner, S. D.; Bohme, D. K. *J. Anal. At. Spectrom.* **2000**, *15*, 1207−1210.

(18) Lee, C. Y.; W.; Parr, R. G. *Phys. Rev. B* **1988**, *37*, 785−789.

(19) Becke, A. D. *J. Chem. Phys.* **1993**, *98*, 5648−5652.

(20) Frisch, M. J.; Trucks, G. W.; Schlegel, H. B.; Scuseria, G. E.; Robb, M. A.; Cheeseman, J. R.; Zakrzewski, V. G.; Montgomery, J. A., Jr.; Stratmann, R. E.; Burant, J. C.; Dapprich, S.; Millam, J. M.; Daniels, A. D.; Kudin, K. N.; Strain, M. C.; Farkas, O.; Tomasi, J.; Barone, V.; Cossi, M.; Cammi, R.; Mennucci, B.; Pomelli, C.; Adamo, C.; Clifford, S.; Ochterski, J.; Petersson, G. A.; Ayala, P. Y.; Cui, Q.; Morokuma, K.; Malick, D. K.; Rabuck, A. D.; Raghavachari, K.; Foresman, J. B.; Cioslowski, J.; Ortiz, J. V.; Stefanov, B. B.; Liu, G.; Liashenko, A.; Piskorz, P.; Komaromi, I.; Gomperts, R.; Martin, R. L.; Fox, D. J.; Keith, T.; Al-Laham, M. A.; Peng, C. Y.; Nanayakkara, A.; Gonzalez, C.; Challacombe, M.; Gill, P. M. W.; Johnson, B. G.; Chen, W.; Wong, M. W.; Andres, J. L.; Head-Gordon, M.; Replogle, E. S.; Pople, J. A. *Gaussian 98*, revision A.11.4; Gaussian, Inc.: Pittsburgh, PA, 1998.

(21) Clark, T.; Chandrasekhar, J.; Spitznagel, G. W.; Schleyer, P. v. R. *J. Comput. Chem.* **1983**, *4*, 294−301.

(22) Krishnan, R.; Binkley, J. S.; Seeger, R.; Pople, J. A. *J. Chem. Phys.* **1980**, *72*, 650−654.

(23) Wadt, W. R.; Hay, P. J. *J. Chem. Phys.* **1985**, *82*, 284−298.

(24) Hay, P. J.; Wadt, W. R. *J. Chem. Phys.* **1985**, *82*, 270−283.

(25) Hay, P. J.; Wadt, W. R. *J. Chem. Phys.* **1985**, *82*, 299−310.

Table 1. Summary of Rate Coefficients for Reactions Observed with Mercury Cations Measured with a SIFT Apparatus in He at 0.35 Torr and 295 K[a]
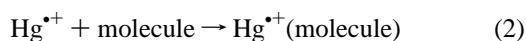
molecule	IE/eV[b]	reaction	k[c]	k/k_c[d]	ΔIE/eV[e]
SF_6	15.3	$Hg^{\bullet+} + SF_6 \rightarrow$ no reaction	$\leq 10^{-13}$	$\leq 1.5 \times 10^{-4}$	4.9
CO	14.0	$Hg^{\bullet+} + CO \rightarrow$ no reaction	$\leq 10^{-13}$	$\leq 1.5 \times 10^{-4}$	3.6
CO_2	13.8	$Hg^{\bullet+} + CO_2 \rightarrow$ no reaction	$\leq 5.0 \times 10^{-13}$	$\leq 7.0 \times 10^{-4}$	3.4
N_2O	12.9	$Hg^{\bullet+} + N_2O \rightarrow$ no reaction	$\leq 10^{-13}$	$\leq 1.4 \times 10^{-4}$	2.5
D_2O	12.6	$Hg^{\bullet+} + D_2O \rightarrow Hg^{\bullet+}(D_2O)$	8.0×10^{-12}	3.9×10^{-3}	2.2
CH_4	12.5	$Hg^{\bullet+} + CH_4 \rightarrow Hg^{\bullet+}(CH_4)$	$\leq 10^{-13}$	$\leq 5.0 \times 10^{-5}$	2.1
CH_3F	12.4	$Hg^{\bullet+} + CH_3F \rightarrow Hg^+(CH_3F)$	2.5×10^{-12}	1.4×10^{-3}	2.0
$^{\bullet}O_2{}^{\bullet}$	12.1	$Hg^{\bullet+} + {}^{\bullet}O_2{}^{\bullet} \rightarrow$ no reaction	$\leq 10^{-13}$	$\leq 1.9 \times 10^{-4}$	1.7
CH_3Cl	11.4	$Hg^{\bullet+} + CH_3Cl \rightarrow Hg^+(CH_3Cl)$	4.0×10^{-11}	0.024	1.0
OCS	11.2	$Hg^{\bullet+} + OCS \rightarrow Hg^{\bullet+}(OCS)$	7.7×10^{-13}	8.0×10^{-3}	0.8
CS_2	10.1	$Hg^{\bullet+} + CS_2 \rightarrow CS_2{}^{\bullet+} + Hg$	9.3×10^{-10}	1.0	−0.3
NH_3	10.1	$Hg^{\bullet+} + NH_3 \rightarrow NH_3{}^{\bullet+} + Hg$	1.2×10^{-9}	0.48	−0.3
C_6F_6	9.9	$Hg^{\bullet+} + C_6F_6 \rightarrow C_6F_6{}^{\bullet+} + Hg$	7.4×10^{-10}	1.0	−0.5
$NO_2{}^{\bullet}$	9.6	$Hg^{\bullet+} + NO_2{}^{\bullet} \rightarrow NO_2{}^+ + Hg$	3.1×10^{-10}	0.42	−0.8
$NO^{\bullet}$	9.3	$Hg^{\bullet+} + NO^{\bullet} \rightarrow NO^+ + Hg$	1.2×10^{-10}	0.19	−1.1
C_6H_6	9.2	$Hg^{\bullet+} + C_6H_6 \rightarrow C_6H_6{}^{\bullet+} + Hg$	6.1×10^{-10}	0.61	−1.1

[a] The reactions are listed in order of increasing exothermicity of electron transfer. [b] Taken from ref 13. [c] In units of cm^3 molecule^{-1} s^{-1}. The estimated uncertainty is ±30%. [d] k/k_c represents the reaction efficiency (see text). [e] ΔIE = IE(Molecule) − IE(Hg).

reported structures are at minima. Zero-point energies (unscaled) and thermal corrections obtained from the calculations were used to determine relative enthalpies at 298 K. Finally, entropy terms were included to obtain relative free energies at 298 K.

4. Results and Discussion

4.1. Kinetic Results. Table 1 summarizes the effective bimolecular rate coefficients obtained for reactions of $Hg^{\bullet+}$ with 16 small molecules, both inorganic and organic. Six of these (CS_2, NH_3, C_6F_6, NO_2, NO, C_6H_6) react by electron transfer, reaction 1, five (D_2O, CH_4, CH_3F, CH_3Cl, OCS) react by ligand association, reaction 2, and five others (SF_5, CO, CO_2, N_2O, O_2) do not show any measurable product formation or reaction, $k \leq 5.0 \times 10^{-13}$ cm^3 molecule^{-1} s^{-1}, under our operating conditions. The ligation reactions are assumed to proceed by termolecular collisional stabilization, although the pressure dependence of the effective bimolecular rate coefficient was not measured.

$$Hg^{\bullet+} + \text{molecule} \rightarrow \text{molecule}^{\bullet+} + Hg \quad (1)$$

$$Hg^{\bullet+} + \text{molecule} \rightarrow Hg^{\bullet+}(\text{molecule}) \quad (2)$$

Representative data for reactions 1 and 2 are shown in Figures 1 and 2. The electron transfer was observed to be terminal in all cases, under our operating conditions, except for the electron transfer from CS_2 to $Hg^{\bullet+}$ which is followed by the association of $CS_2{}^{\bullet+}$ with CS_2 to form the dimer ion $(CS_2)_2{}^{\bullet+}$, as shown in Figure 1. The primary association reaction 2 was followed by a secondary association reaction in all cases except with methane.

Also included in Table 1 are values for the reaction efficiencies. The reaction efficiency is taken to be equal to the ratio k/k_c where k is the experimentally measured rate coefficient and k_c is the capture or collision rate coefficient computed using the algorithm of the modified variational transition-state/classical trajectory theory developed by Su and Chesnavich.[26]

4.2. Trends with Exothermicity. Table 1 includes values for the overall energy change for electron transfer, ΔIE, and
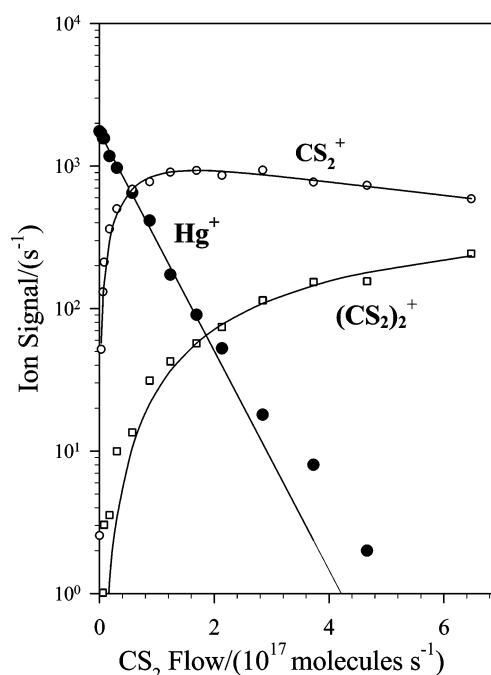

Figure 1. Ion profiles recorded for the reactions initiated by $Hg^{\bullet+}$ with carbon disulfide added into the flow tube flushed with helium buffer gas at 0.35 Torr and 295 K. The slight curvature in the data observed after a linear decay of almost 2 orders of magnitude is attributed to a small background.

these indicate that electron transfer to $Hg^{\bullet+}$ is exothermic only with six of the molecules investigated (CS_2, NH_3, C_6F_6, NO_2, $NO^{\bullet}$, and C_6H_6). The efficiencies for these electron transfers are generally ≥ 0.4 except with NO for which $k/k_c = 0.19$. We have recently discussed the possible origin for the low observed efficiency of electron transfer from $NO^{\bullet}$ to $Hg^{\bullet+}$ in terms of the low Franck−Condon factor associated with the near-resonant ionization of NO.[27] The actual order in the magnitudes of the efficiencies of all the six electron-transfer reactions that were observed cannot be rationalized in a straightforward fashion. At thermal energies ($E_{cm} \ll$ 1 eV), neither the Franck−Condon model, energy resonance, nor statistical energy partitioning alone provides a general

(26) Su, T.; Chesnavich, W. J. *J. Chem. Phys.* **1982**, *76*, 5183−5185.

(27) Jarvis, M. J. Y.; Blagojevic, V.; Koyanagi, G. K.; Bohme, D. K. *Chem. Phys. Lett.* **2005**, *416*, 268−271.
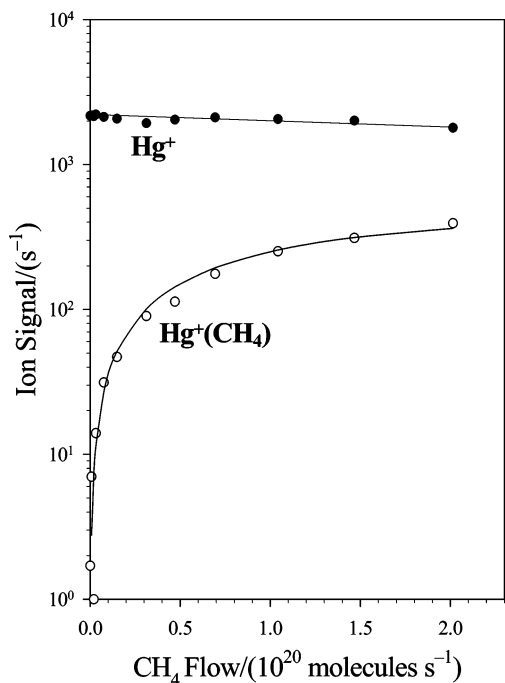
Figure 2. Ion profiles recorded for the reactions initiated by $Hg^{\bullet+}$ with methane added into the flow tube flushed with helium buffer gas at 0.35 Torr and 295 K.

rule for deciding the efficiency of electron transfer,[28] especially for electron-transfer systems involving larger molecules with additional nuclear degrees of freedom that can increase the density of states at near-resonant energies, as well as adding nuclear coordinates along which electron-transfer transitions can occur.[29]

The interactions between $Hg^{\bullet+}$ and molecules with IE (molecule) > IE (Hg) are much less efficient and result in ligand association or do not lead to observable products (see Table 1). No products were observed with the diatomic molecules CO and O_2, the two triatomic molecules CO_2 and N_2O (these triatomic molecules have low polarizabilities and dipole moments), and SF_6.

Figure 3 provides an overview of the dependence of the efficiency for the apparent bimolecular reactions on ΔIE.

4.3. Equilibrium Kinetics and Standard Free Energies of Ligation. Equilibrium kinetics were explored for the association reactions with the five ligands D_2O, CH_4, CH_3F, CH_3Cl, and OCS. The ion-signal ratio plots were nicely linear for the ligation reactions of $Hg^{\bullet+}$ with OCS and CH_4 (see Figure 4). Equilibrium also was well defined for the second additions of CH_3F and CH_3Cl. Table 2 lists the equilibrium constants that were measured. Also included in Table 2 are the standard free energies of ligation that were derived from $\Delta G^\circ = -RT \ln K$ at 295 K and these have values in the range from -5.4 to -9.3 kcal mol^{-1}.

The interaction of $Hg^{\bullet+}$ with methane appears as the weakest and that with CH_3Cl the strongest, although the relative position of D_2O is uncertain. When two additions

(28) Kato, S. *The encyclopedia of mass spectrometry. Vol. 1, Theory and ion chemistry*; Elsevier Science: Boston, 2003; p 284.
(29) Dressler, R. A.; Viggiano, A. A. *The encyclopedia of mass spectrometry. Vol. 4, Fundamentals of and Applications to Organic (and Organometallic) Compounds*; Elsevier Science: Boston, 2005; p 538.
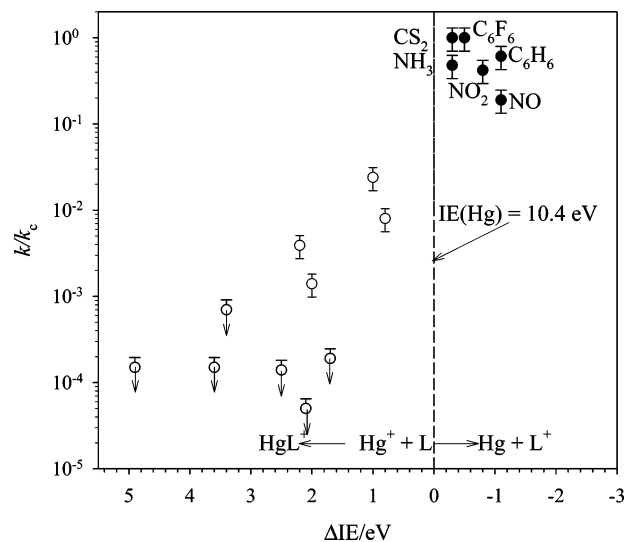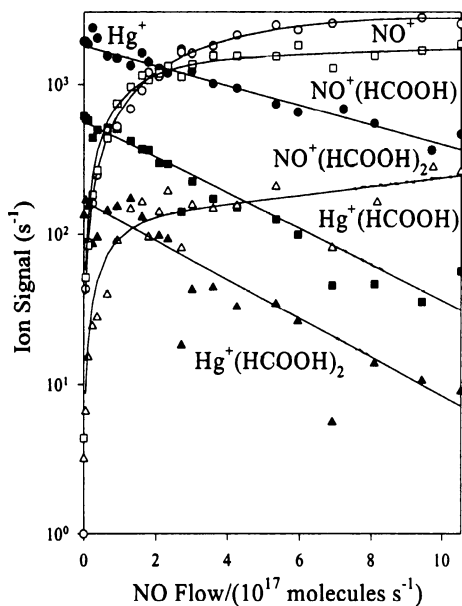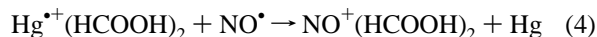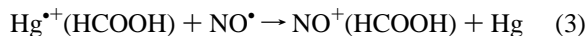
Figure 3. Dependence of the apparent bimolecular efficiency for reactions of $Hg^{\bullet+}$ ions with various molecular ligands, L, on $\Delta IE = IE(L) - IE(Hg)$. The ligands that transfer an electron to $Hg^{\bullet+}$ are labeled.
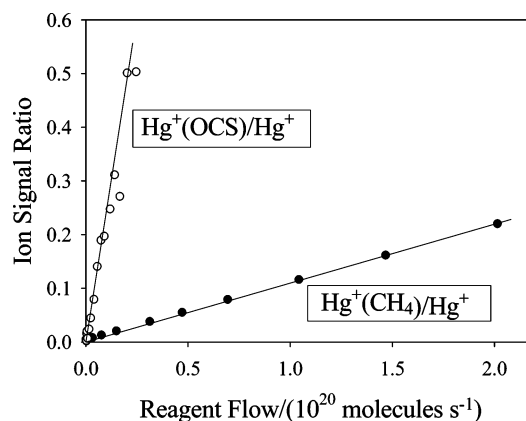
Figure 4. Ion signal ratio plots demonstrating the attainment of equilibrium for the association of methane and carbonyl sulfide to $Hg^{\bullet+}$ in helium buffer gas at 0.35 Torr and 295 K.

Table 2. Summary of Equilibrium Results for the Addition of Small Molecules to $Hg^{\bullet+}$ in He at 0.35 Torr and 295 K

equilibrium ligation	K^a	$\Delta G^{\circ\ b}$
$Hg^{+\bullet}+D_2O \leftrightarrow Hg^{+\bullet}(D_2O)$	$\geq 5.1 \times 10^5$	≤ -7.7
$Hg^{+\bullet}(D_2O) + D_2O \leftrightarrow Hg^{+\bullet}(D_2O)_2$	$\geq 1.4 \times 10^5$	≤ -7.0
$Hg^{+\bullet}+CH_4 \leftrightarrow Hg^{+\bullet}(CH_4)$	9.7×10^3	-5.4
$Hg^{+\bullet}+CH_3F \leftrightarrow Hg^{+\bullet}(CH_3F)$	$\geq 2.9 \times 10^5$	≤ -7.4
$Hg^{+\bullet}(CH_3F)+CH_3F \leftrightarrow Hg^{+\bullet}(CH_3F)_2$	2.3×10^4	-5.9
$Hg^{+\bullet}+CH_3Cl \leftrightarrow Hg^{+\bullet}(CH_3Cl)$	$\geq 7.3 \times 10^6$	≤ -9.3
$Hg^{+\bullet}(CH_3Cl)+CH_3Cl \leftrightarrow Hg^{+\bullet}(CH_3Cl)_2$	2.1×10^6	-8.5
$Hg^{+\bullet}+OCS \leftrightarrow Hg^{+\bullet}(OCS)$	1.9×10^5	-7.2

^{a} Standard state = 1 bar. The uncertainty is estimated to be $\pm 30\%$. ^{b} In units of kcal mol^{-1}. The uncertainty is estimated to be less than ± 2 kcal mol^{-1}.

are observed, as is the case with D_2O, CH_3F, and CH_3Cl, the second interaction appears to be weaker, except perhaps in the case of D_2O.

4.4. Solvated Electron Transfer. A few experiments were performed in which formic acid vapor was introduced upstream into the flow tube and the solvated ions $Hg^{\bullet+}(HCOOH)_{1,2}$ were seen downstream. No reactions were observed with CO, CO_2, and O_2, $k < 1 \times 10^{-12}$ cm^3 molecule^{-1} s^{-1}. However, two solvated electron-transfer

Figure 5. Ion profiles recorded for the reactions initiated by $Hg^{\bullet+}(HCOOH)_{0,1,2}$ with HCOOH added upstream and NO added downstream into the flow tube flushed with helium buffer gas at 0.35 Torr and 295 K.

reactions, reactions 3 and 4, were observed with NO in the presence of the bare $Hg^{\bullet+}$ ion reaction (see Figure 5).

$$Hg^{\bullet+}(HCOOH) + NO^{\bullet} \rightarrow NO^{+}(HCOOH) + Hg \quad (3)$$

$$Hg^{\bullet+}(HCOOH)_2 + NO^{\bullet} \rightarrow NO^{+}(HCOOH)_2 + Hg \quad (4)$$

There is some uncertainty in the product distribution of reactions 3 and 4 since the formation of product ions less solvated than those indicated in each case cannot be completely ruled out, nor can the solvation of the NO^{+} product with the HCOOH added to the flow tube. The rate coefficients derived for the loss of $Hg^{\bullet+}(HCOOH)$ and $Hg^{\bullet+}(HCOOH)_2$ are $k_3 = 1.5 \times 10^{-10}$ cm^3 molecule^{-1} s^{-1} and $k_4 = 1.6 \times 10^{-10}$ cm^3 molecule^{-1} s^{-1}. These results are interesting since the rate coefficients for electron transfer to the solvated $Hg^{\bullet+}(HCOOH)_{1,2}$ ions are larger than that for electron transfer to the nonsolvated, bare $Hg^{\bullet+}$ for which $k = 1.2 \times 10^{-10}$ cm^3 molecule^{-1} s^{-1}. Therefore, these experiments indicate that the rate coefficient for electron transfer increases with solvation. This is an interesting result since it runs counter to previous trends in the kinetics reported for other ion/molecule reactions with increasing solvation and may have to do with a favorable shift in energy resonance or the Franck−Condon factors in the ionization of NO.[27,30]

4.5. Computed Structures for Ligated $Hg^{\bullet+}$. Detailed DFT calculations were performed in order to obtain a better understanding of the interactions between $Hg^{\bullet+}$ and various ligands investigated. Table 3 provides the calculated ligand geometries, $Hg^{\bullet+}$(ligand) geometries, Mulliken charges, frontier orbitals of the ligands, and the overlapping orbitals in $Hg^{\bullet+}$−ligand complexes. In all of these systems, except for $Hg^{\bullet+}(O_2)$, the SOMO (singly occupied molecular orbital) is an antibonding orbital that is essentially an sp-hybridized

6s orbital largely on $Hg^{\bullet+}$. In the case of $Hg^{\bullet+}(CH_3F)$, $Hg^{\bullet+}(SF_6)$, and $Hg^{\bullet+}(CO_2)$, orbital analysis shows that there is no other molecular orbital with significant overlap between the $Hg^{\bullet+}$ orbital and the molecular orbitals of the ligands. The orientation of $Hg^{\bullet+}$ in these three complexes is controlled by the electrostatic interaction and the calculations show that $\angle HgFC$, $\angle HgFS$, and $\angle HgOC$ are 180°. In the other $Hg^{\bullet+}-$ ligand complexes, there is an overlapping HOMO-1 orbital, except for $Hg^{\bullet+}(O_2)$ and $Hg^{\bullet+}(CH_3Cl)$ in which the overlapping orbitals are SOMO and HOMO-2, respectively (see Table 3). These overlapping orbitals control the orientation of $Hg^{\bullet+}$ and thus determines the geometry of the $Hg^{\bullet+}-$ ligand complex. The HOMO of CO is along the O−C bond, and it is mainly composed of 2s and $2p_z$ of C and a small fraction of $2p_z$ of O. This results in a higher overlapping in $Hg^{\bullet+}$−CO and lower overlapping in $Hg^{\bullet+}$−OC and thus a stronger bond in $Hg^{\bullet+}$−CO than that in $Hg^{\bullet+}$−OC. This is in line with the proton affinities of CO at C (142.0 kcal mol^{-1}) and O (101.9 kcal mol^{-1}).[31] In $Hg^{\bullet+}$−O_2 and $Hg^{\bullet+}-$ N_2O, The 6s orbital of $Hg^{\bullet+}$ overlaps with the π^*-like HOMO of O_2 and N_2O and gives rise to bent structures for $Hg^{\bullet+}-$ O_2 ($\angle Hg-O-O = 129°$) and $Hg^{\bullet+}-N_2O$ ($\angle Hg-O-N = 140°$). The spatially more extended p orbitals of S facilitate preferred interactions with the sulfur atom instead of the O atom in OCS. The overlapping of the 6s of $Hg^{\bullet+}$ and the 3p of sulfur gives a bent $Hg^{\bullet+}$−SCO complex ($\angle Hg-S-C = 101°$). This is similar to the protonation of OCS.[32,33] The three frontier orbitals of CH_4 have the same symmetry, as shown in Table 3. However, the attempt to find the $Hg^{\bullet+}-$ CH_4 with C_{2v} symmetry was unsuccessful. The stable $Hg^{\bullet+}-$ CH_4 has a C_{3v} geometry in which the 6s orbital of $Hg^{\bullet+}$ overlaps with a hybrid orbital composed of the $2p_z$ orbital of C and the s orbitals of four H atoms. H_2O has a π-like HOMO, and this is not suitable for overlapping with 6s of $Hg^{\bullet+}$. The orbital analysis of $Hg^{\bullet+}$−H_2O indicates that 6s of $Hg^{\bullet+}$ overlaps with HOMO-1 of H_2O to form a planar $Hg^{\bullet+}-$ H_2O complex. Cl (with its occupied p orbital) has a bigger atomic radius and lower electronegativity than F, and this facilitates donation of an electron to $Hg^{\bullet+}$, formation of a SOMO, and side-on C−Cl bonding rather than end-on electrostatic bonding as is the case with CH_3F. In $Hg^{\bullet+}-$ HCOOH, the 6s of $Hg^{\bullet+}$ overlaps with the π^*-like HOMO of HCOOH to give a planar complex.

4.6. Computed Energetics for Ligation. The calculated values for $\Delta H_0°$, $\Delta H_{298}°$, and $\Delta G_{298}°$ for the association reactions of $Hg^{\bullet+}$ with different ligands are listed in Table 4. The interactions between $Hg^{\bullet+}$ and the various ligands generally are weak. The calculated values of $\Delta H_{298}°$ and $\Delta G_{298}°$ for the first ligand addition are predicted to be in the range from −6.7 and −1.2 kcal mol^{-1}, respectively, for $Hg^{\bullet+}(OC)$ to −28.4 and −21.7 kcal mol^{-1}, respectively, for
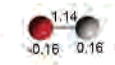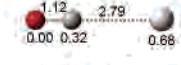
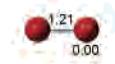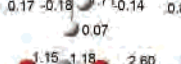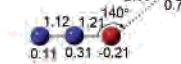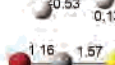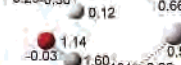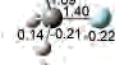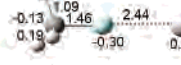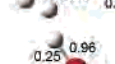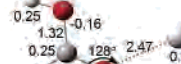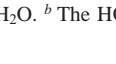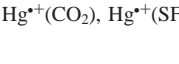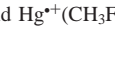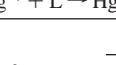(30) Bohme, D. K. *Ionic Processes in the Gas Phase*; Reidel Publishing Co.: Dordrecht, 1982.
(31) Hunter, E. P.; Lias, S. G. *J. Phys. Chem. Ref. Data* **1998**, *27*, 413−656.
(32) Saebo, S.; Sanz, M. M.; Foster, S. C. *Theor. Chem. Acc.* **1997**, *97*, 271−276.
(33) Scarlett, M.; Taylor, P. R. *Chem. Phys.* **1986**, *101*, 17−26.

Table 3. Geometries (Bond Distances in Å), Mulliken Charges, and Frontier Molecular Orbitals of Ligands and Hg$^{•+}$(ligand) Complexes

Ligand	HOMO of Ligand [a]	Complex	Overlap Orbital [b]

(CO, O$_2$, SF$_6$, CO$_2$, N$_2$O, CH$_4$, OCS, CH$_3$F, CH$_3$Cl, H$_2$O, HCOOH)

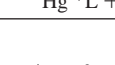[a] The HOMO-1 is shown for CH$_3$Cl and H$_2$O. [b] The HOMOs are given for Hg$^{•+}$(CO$_2$), Hg$^{•+}$(SF$_6$), and Hg$^{•+}$(CH$_3$F) in which there are no overlapping orbitals.

Table 4. Calculated Values of $\Delta H_0°$, $\Delta H_{298}°$ and $\Delta G_{298}°$ (All in kcal mol^{-1}) for Reactions of the Types Hg$^{•+}$ + L → Hg$^{•+}$L and Hg$^{•+}$L + L → Hg$^{•+}$L$_2$

| | Hg$^{•+}$ + L → Hg$^{•+}$L | | | | Hg$^{•+}$L + L → Hg$^{•+}$L$_2$ | | | |
| | | | $\Delta G_{298}°$ | | | | $\Delta G_{298}°$ | |
L	$\Delta H_0°$	$\Delta H_{298}°$	calcd	exptl	$\Delta H_0°$	$\Delta H_{298}°$	calcd	exptl
CO(at O)	−6.6	−6.7	−1.2					
CO(at C)	−12.2	−12.4	−6.5					
O$_2$	−7.0	−7.4	−2.0					
SF$_6$	−8.1	−7.9	−3.3					
CO$_2$	−11.4	−11.4	−6.1					
N$_2$O	−11.9	−12.1	−6.8					
CH$_4$	−8.8	−9.1	−4.5	−5.4	−4.4	−5.4	3.7	
OCS	−16.1	−16.3	−11.2	−7.2	−7.3	−6.6	−1.5	
CH$_3$F	−19.8	−19.8	−14.6	≤ −7.4	−14.5	−13.8	−9.0	−5.9
CH$_3$Cl	−22.3	−22.4	−17.3	≤ −9.3	−12.7	−11.9	−7.1	−8.5
H$_2$O	−25.0	−25.6	−20.0		−16.7	−16.6	−10.3	
D$_2$O	−25.2	−26.7	−20.0	≤ −7.7	−17.0	−17.0	−10.3	≤ −7.0
HCOOH	−28.1	−28.4	−21.7		−14.5	−13.8	−6.5	
HCOOH	−29.2[a]	−29.4[a]	−20.8[a]		−14.9[b]	−14.3[b]	−6.8[b]	

[a] For NO$^+$ + HCOOH → NO$^+$(HCOOH). [b] For NO$^+$(HCOOH) + HCOOH → NO$^+$(HCOOH)$_2$.

Hg$^{•+}$(HCOOH). The values of $\Delta H_{298}°$ and $\Delta G_{298}°$ for the second ligand addition are in the range from −5.4 and 3.7 kcal mol^{-1}, respectively, for CH$_4$ to −17.0 and −10.3 kcal mol^{-1}, respectively, for D$_2$O. These computed results are in line with our experimental observations. There is agreement in the absolute values for methane, within experimental error,

but the experimental value of -7.2 ± 2 kcal mol^{-1} for OCS is slightly lower than the predicted value of -11.2 kcal mol^{-1}.

Our failure to observe the first association products of CO, O_2, SF_6, CO_2, and N_2O, and the second association products of CH_4 and OCS can be explained by the low $\Delta G_{298}°$ predicted by theory for these association reactions. Weak bonding leads to low rates of ligation since the lifetime of the association intermediate decreases with decreasing bond strength[33] and it also leads to a greater probability of breakup in the sampling. $Hg^{•+}(CH_4)$ appears to be an exception since it was observed to be formed even though the $\Delta G_{298}°$ for $Hg^{•+}(CH_4)$ formation is only -5.4 kcal mol^{-1} and so is lower than that for CO, CO_2, and N_2O. However, $Hg^{•+}(CH_4)$ formation is kinetically more favorable since the larger number of degrees of freedom in CH_4 leads to a longer lifetime for the association intermediate.[34]

The strongest interaction predicted by theory is that between $Hg^{•+}$ and HCOOH in $Hg^{•+}(HCOOH)$, and this can be attributed to the bent HCOOH structure in which $Hg^{•+}$ interacts primarily with the HOMO of HCOOH and less so electrostatically with the hydroxyl oxygen. The strong interaction between $Hg^{•+}$ and H_2O in $Hg^{•+}(H_2O)$ can be attributed to the large overlap between the 6s orbital of $Hg^{•+}$ and the HOMO-1 of H_2O. The interaction between $Hg^{•+}$ and CH_3Cl in $Hg^{•+}(CH_3Cl)$ also is due to orbital overlapping and results in a lower $\Delta H_{298}°$ compared to that in $Hg^{•+}(H_2O)$. Only Coulombic interaction was seen in $Hg^{•+}(CH_3F)$, so that a lower $\Delta H_{298}°$ was obtained compared to that for $Hg^{•+}(CH_3Cl)$ and $Hg^{•+}(H_2O)$. The high ability of the sulfur 3p orbital in OCS to extend spatially results in effective overlap with the 6s orbital of $Hg^{•+}$. This leads to a higher interaction between OCS and $Hg^{•+}$ compared to those with O_2, N_2O, CO_2, and CO in which the oxygen, nitrogen, and carbon atoms have small atomic radii and a lower ability for spatial extension. It is easy to understand the lower interaction with CH_4, which has a symmetric geometry and no dipole moment. The lower $\Delta H_{298}°$ for the second association can be attributed to charge delocalization by the first ligand which reduces the electrostatic interaction compared to that with the bare charge-localized $Hg^{•+}$.

A plot of the calculated $Hg^{•+}$ affinity vs proton affinity is shown in Figure 6. There is an obvious correlation between the $Hg^{•+}$ affinity and the proton affinity, except with CH_4 and SF_6. The larger atomic radius of $Hg^{•+}$ prevents a close approach to the ligand and this, together with the lower total overlap with the diffuse 6s^1 orbital of $Hg^{•+}$, contribute to a generally much lower $Hg^{•+}$ affinity compared to the proton affinity. $Hg^{•+}$ binds less tightly than H^+ since the 6s^1 orbital of $Hg^{•+}$ is occupied and the 1s^0 of H^+ is not.

The exceptions for CH_4 and SF_6 can be attributed to differences in the nature of the bonding of $Hg^{•+}$ and H^+ with these two molecules. Previous experimental and theoretical studies[35–40] suggest that protonated CH_4 has a C_s symmetry
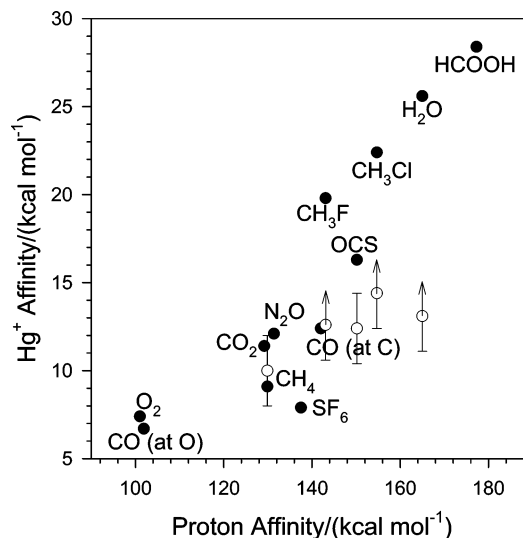

Figure 6. Correlation between the computed $Hg^{•+}$ affinities and the proton affinities reported in ref 31. The solid circles show the calculated values, and the open circles show the affinities derived from values for $\Delta G°$ based on our equilibrium constant measurements and computed values for $\Delta S°$.

with a CH_3 tripod and a 3-center, 2-electron CH_2 structure. All of the five H atoms in CH_5^+ coordinate with carbon atom. This results in a high proton affinity of 129.9 kcal mol^{-1}.[31] Our computed structure for $Hg^{•+}(CH_4)$ is quite different: the direct bonding of $Hg^{•+}$ to C is energetically unfavorable. All attempts at the B3LYP/6-311++G(d,p) level to find stable protonated SF_6, SF_6H^+, in which the proton interacts with one, two, or three fluorine atoms were not successful; SF_5^+··· FH was found to be the unique stable structure instead. However, the analogous SF_5^+···FHg species was found not to exist; the complex $Hg^{•+}(SF_6)$ is the stable structure of the adduct of $Hg^{•+}$ and SF_6.

The absolute accuracy of the computed values of the ligation energies are difficult to assess because of the significant difference in the quality of the basis sets used in the calculations for Hg and the other elements. Theory and experiment agree on the standard free energy of ligation for the addition of the first ligand, at least within the uncertainties of, and limits to, the measurements, and the reduction in the free energy of ligation for the second ligand that was observed with D_2O, CH_3F, and CH_3Cl. The $Hg^{•+}$ affinities derived from values for $\Delta G°$ based on our equilibrium constant measurements and computed values for $\Delta S°$ are included in Figure 6 and provide a quick overview of the agreement between theory and experiment.

Also of interest is the theoretical prediction of the change in enthalpy for the electron transfer from NO with increasing HCOOH solvation, reactions 3 and 4. IE(Hg) is reduced by 1.22 and 1.85 eV with the addition of one and two molecules of HCOOH, respectively, if the interaction of Hg with HCOOH is neglected. $\Delta H_{298}°$ for electron-transfer shifts by -0.043 and -0.065 eV with the addition of one and two

(34) Good, A. *Chem. Rev.* **1975**, *75*, 561–583.
(35) Marx, D.; Parrinello, M. *Sci.* **1999**, *284*, 59, 61.
(36) Schleyer, P. v. R.; Carneiro, J. W. d. M. *J. Comput. Chem.* **1992**, *13*, 997–1003.

(37) Novoa, J. J.; Tel, L. M. *An. Quim., Ser. A* **1985**, *81*, 155–159.
(38) Wang, B.; Hou, H. *J. Phys. Chem. A* **2005**, *109*, 8537–8547.
(39) Schreiner, P. R. *Angew. Chem., Int. Ed.* **2000**, *39*, 3239–3241.
(40) Huang, X.; McCoy Anne, B.; Bowman Joel, M.; Johnson Lindsay, M.; Savage, C.; Dong, F.; Nesbitt David, J. *Science* **2006**, *311*, 60–63.

molecules of HCOOH, respectively, to $Hg^{\bullet+}$ and NO^+, according to reactions 3 and 4.

5. Conclusions

The mercury radical cation, $Hg^{\bullet+}$, accepts an electron with high efficiency ($>19\%$) in the gas phase at room temperature from molecules with ionization energies lower than its recombination energy. Molecules with higher ionization energies will associate with $Hg^{\bullet+}$ with affinities that correlate with proton affinities but are much smaller due primarily to the larger size and electron occupancy of the diffuse $6s^1$ orbital of $Hg^{\bullet+}$. Methane and SF_6 are special cases in that these two molecules interact with a proton and $Hg^{\bullet+}$ in distinctly different ways. Theory indicates that the attractive interactions between $Hg^{\bullet+}$ and the CH_3F, SF_6, and CO_2 ligands are electrostatic in their corresponding adduct ions whereas the 6s orbital of $Hg^{\bullet+}$ overlaps with the frontier orbital (HOMO or HOMO-1) of the ligand in the other $Hg^{\bullet+}-$ligand complexes that were investigated. This overlap controls the orientation of $Hg^{\bullet+}$ and thus determines the geometry of the $Hg^{\bullet+}-$ligand complex. The ease of observation of ligated $Hg^{\bullet+}$ under our experimental operating conditions appears to be determined both by the strength of the interaction in the ligated complex and the number of atoms in the ligand. Of the diatomic and triatomic ligands, only carbonyl sulfide and water were observed to add to $Hg^{\bullet+}$: these additions have computed $\Delta G_{298}°$'s more negative than -11 kcal mol^{-1}. The five-atom ligands CH_4, CH_3F, CH_3Cl, and HCOOH were observed to add with computed $\Delta G_{298}°$'s more negative than only -4 kcal mol^{-1}. SF_6 was not observed to add and this addition has the lowest $\Delta G_{298}°$ of -3.3 kcal mol^{-1}. $Hg^{\bullet+}(ligand)_2$ formation was observed with D_2O, CH_3F, CH_3Cl, and HCOOH with computed $\Delta G_{298}°$'s more negative than only -4 kcal mol^{-1}. The experimental values, or limiting values, of $\Delta G_{298}°$ deduced from measurements of equilibrium constants is reproduced by the calculations.